Materials Characterization 206 (2023) 113402

Contents lists available at ScienceDirect

Materials Characterization

journal homepage: www.elsevier.com/locate/matchar

Point excess solute: A new metric for quantifying solute segregation in atom probe tomography datasets including application to naturally aged solute clusters in Al-Mg-Si-(Cu) alloys

J.R. Famelton [a,b,*], C.A. Williams [c], C. Barbatti [d], P.A.J. Bagot [a], M.P. Moody [a]

[a] Department of Materials, University of Oxford, Oxford, UK
[b] Brunel Centre for Advanced Solidification Technology, Brunel University, London, UK
[c] Innoval Technology Ltd, Banbury, UK
[d] Constellium University Technology Centre, Brunel University, London, UK

ARTICLE INFO

Keywords:
Solute cluster
Atom probe tomography
Natural ageing
Al-Mg-Si-Cu

ABSTRACT

Accurate, repeatable and quantitative analysis of nanoscale solute clustering in atom probe tomography (APT) datasets is a complex challenge which is made more difficult by the positional uncertainty and lack of absolute resolution inherent to the technique. In this work a new method, the point excess solute, is introduced for quantifying solute segregation in datasets with limited spatial resolution. This new method is based on measuring the matrix concentration using a dataset sampling method. We show the new method can accurately reproduce the values expected from synthetic datasets a priori and when the dataset spatial resolution and or phase contrast is too low for accurate quantification this is observable. The method is then applied to naturally aged solute clusters in the Al-Mg-Si-Cu system. Datasets were collected with a range of natural ageing times from 8 min to 76 weeks. The formation of the solute clusters is shown to be unaffected by the Cu content of the alloy.

1. Introduction

Atom probe tomography (APT) is widely used for the detection and characterisation of features of fine-scale chemical segregation termed solute clusters in a range of materials [1–5]. APT generates nano-scale chemical information in the form of atomic reconstructions, which are 4 dimensional data, with each point in the 3D data having a Cartesian coordinate and a mass-to-charge-state ratio. From the mass-to-charge-state ratio a chemical identity can be assigned to each point creating a point cloud of data from which features of chemical segregation can be identified.

In this work we will use a broad definition for a solute cluster that is relevant for APT data; while other definitions may be more specific and include structural and ordering requirements [2]. As this information is often absent from APT data it cannot be included as part of the definition. Here we treat true solute clusters as being discrete regions in the APT data with a concentration of one or more elements above that of the concentration of these elements in a surrounding matrix. In this definition, the atoms of the clustering elements in the surrounding matrix have no spatial correlation to themselves or other clustering elements. The matrix can be described as a random solid solution (RSS). Across previous works, different methods of selecting such regions of solute segregation from APT data are themselves the definition of a solute cluster within the study for which that method is being used.

Methods used for extraction of features classed as solute clusters by this definition, include the commonly used DBSCAN algorithm (of which maximum separation algorithm is a specialised case) and iso-concentration surfaces, generated from de-localised concentration fields. Other less commonly applied methods have been based on Delaunay tessellations and Voronoi cells [6,7], using isolated solute ions [8] and radial distribution functions [9,10]. More recently more advanced algorithms and machine learning principles have also been applied to APT data [11–14].

A common source of complications to several solute cluster identification methods is the selection of parameters which determine the cut-off between clustered and non-clustered regions of the dataset. These parameters can have large effects on the extract distribution of cluster properties [15]. Inconsistent parameter selection between operators can lead to poor repeatability and comparability of results and some parameters will provide results which are inaccurate and far from the true

* Corresponding author at: Department of Materials, University of Oxford, Oxford, UK.
E-mail address: james.famelton@brunel.ac.uk (J.R. Famelton).

https://doi.org/10.1016/j.matchar.2023.113402
Received 3 May 2023; Received in revised form 11 September 2023; Accepted 15 October 2023
Available online 18 October 2023

cluster characteristics [15]. As such several works have tried to determine ways of automatically or semi-automatically selecting parameters to produce more accurate, repeatable and comparable results, [7,8,16–20].

In APT data, the atomic density of solute ions residing within the true clusters will cover a range of values. However, the distribution of values can overlap with the distribution of atomic densities of solute residing with the matrix. This can become problematic when selecting a single cut off density value to delineate clustered ions from those in the matrix. As such methods that select solute clusters based on global cut-offs in density [7,16,17,19,20] may not accurately characterise the dataset. Alternative methods have been suggested to extract features over a range of densities [12–14] and perhaps offer the best potential for accurately determining the number of true solute clusters a dataset. Some methods [12,14] do still require input of user selected parameters and can struggle to accurately quantify the solute clustering in a dataset when the solute density contrast between clusters and matrix is low.

No matter the methods used for extracting solute clusters however, there are also limitations to accuracy that occur for measurements at the smallest length scale of solute segregation, due to the finite spatial resolution of the APT evaporation process and reconstruction [10]. This leads to uncertainty in size and spatial overlap between original cluster and matrix ions, such that there is a loss of compositional information [10]. Due to this overlap in the APT reconstruction the primary matrix element(s) are often not considered as part of cluster composition and only ratios of the segregating solute species are quoted [2], although this ratio can still be influenced by spatial overlap if the ratio of segregating elements was different between the cluster and matrix.

In this work we propose a method to extract quantitative information from the APT dataset when the ability to resolve solute clusters is limited, either due to poor spatial resolution arsing from experimental measurement limitations or due to the inherently small scale segregation and low concentration contrast nature of the clusters, or a combination of these factors. The method is free from user-defined parameters and is hence consistent and repeatable between different operators and provides results which are directly comparable between different datasets and material treatments. The new method is validated against synthetic APT data, with known cluster characteristics, and a case study of the method applied to the early stages of solute cluster development during room temperature ageing of Al-Mg-Si-(Cu) alloys is presented.

2. Point excess method

Fig. 1a shows a theoretical schematic of the solute concentration profile measured across two regions, comprising 50 at.% and 10 at.% solute in the cluster and matrix regions respectively. The black solid line shows an idealised case, where there is a sharp interface. The blue dotted line indicates a more realistic scenario, where due to poor identification of which region an ion was originally from and/or interface blurring due to spatial aberrations in the APT reconstruction, the solute concentration is no longer bimodal. In no section is the measured concentration the same as the original cluster solute concentration, c_c. Without making assumptions about the nature of this blurring, the core composition of the cluster cannot be directly measured. In this situation what is however not lost is the matrix concentration, c_m, which can accurately measured at distances sufficiently far from the interface. In an analogous manner to the calculation of a Gibbsian interfacial excess [21,22], the number of solute ions in excess of the base matrix concentration can be calculated, here referred to as the point excess solute, Ψ. These excess solute ions may be part of a small volume of high concentration clusters, or a larger volume of lower concentration clusters. The parameter is defined such that the value of Ψ can be used as a quantification for the amount of solute segregation when the characteristics, cluster solute concentration and volume fraction, cannot be measured.

In order to calculate Ψ, the point cloud of ions needs to be linearly indexed from the ions thought most likely to be part of a solute cluster, to the least likely to be part of a solute cluster. The choice of how to index the dataset will be addressed in detail below. The cumulative sum of solute ions, from most likely to be clustered to least likely, as a function of the cumulative sum of all ions can be plotted from this, as shown schematically in Fig. 1b. The value of Ψ is defined as the y-axis intercept of a linear fit to the section of this graph where the gradient, i.e. concentration, is constant. The measured value of Ψ is a number of ions, which will depend on the size of the dataset measured and the total dataset concentration of solute. It can be normalised by dividing by the total number of solute ions observed, to give the value Ψ_n, which leads to the following expressions,

$$\Psi_n = \Psi / N_s \tag{1}$$

$$\Psi_n = 1 - c_m / c_t \tag{2}$$

where; N_s, is the total number of solute ions in the dataset; c_m is the concentration of solute in the matrix and c_t, is the total dataset concentration of solute; $c_t = N_s/N_t$. N_t is the total number of ions in the dataset. Eq. (2) is derived from considering that Ψ is equivalent to $N_s - c_m N_t$, the number of solute ions above a base matrix concentration.

If the blurring of cluster and matrix regions is sufficient that no section of the dataset which has the starting matrix composition can be identified, then this measurement also breaks down. This situation is demonstrated by the red dashed lines in Fig. 1. If the length scales of

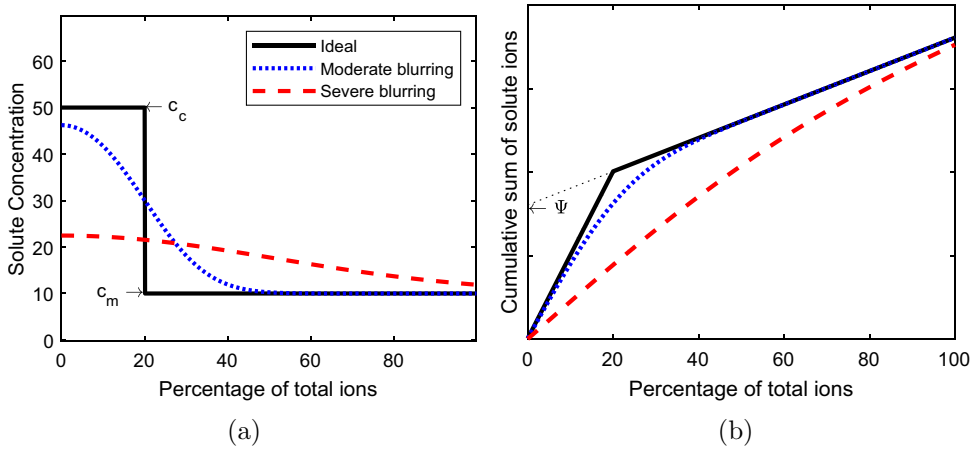

Fig. 1. a) Solute concentration profiles moving from cluster to matrix region with theoretical compositions, c_c and c_m respectively. Volume is represented by percentage of total ions. In this example clusters take up 20% of the volume. For moderate blurring matrix concentration is still measurable, but not with severe blurring. b) Same situation as in a) but for cumulative sum of solute ions. The excess solute, Ψ, is measurable for moderate blurring but not severe blurring.

segregation are small compared to positional uncertainty, complete overlap between original clusters and matrix may occur.

2.1. Dataset sampling methodology

Whether a uniform matrix concentration can be resolved will be influenced by the method used to linearly index the dataset, as well as positional overlap and aberrations within the reconstruction. In this work only one method for indexing the dataset is applied, but the principle of calculating Ψ can be generalised to other methods. In this work the dataset is indexed using an adapted maximum separation approach.

In the maximum separation method, the dataset is categorised into solute ions and non-solute ions, with a solute ion considered to be clustered if it is within a distance d_{max} of another solute ion [18,23]. Non-solute ions can be added to the clusters if they are within a distance d_{inc} of a clustered solute ion [24]. d_{inc} is sometimes referred to as L. Here we do not consider the additional step of erosion [24]. It should be noted that the terms solute and non-solute used here, refer to how the ion is categorised as an input to the maximum separation algorithm and that the non-solute category can contain ions which from a chemistry point of view would be called solute ions.

In the new dataset sampling methodology, the data is separated such that some of the solute ions are used to index the dataset, while a random sample of them are used for the calculation of Ψ. Firstly a fixed fraction of the solute ions in the dataset are selected (Fig. 2). These ions are reassigned a new, unique mass-to-charge-state ratio and a new identity; Q. A sampling of the non-solute ions is also made, the sampling fraction being the same as the fraction of solute ions now assigned as Q. Among the non-solute ions each ionic species is sampled equally. The rest of the non-solute ions are temporarily discarded. A combined dataset is then made of the non-sampled solute, the Q ions i.e. the sampled solute, and the sampled non-solute ions (Fig. 2). The selection parameter d_{max} and alongside it the inclusion parameter $d_{inc} = d_{max}$, are incrementally increased from 0. This leads to shells of Q and sampled non-sample ions being selected around regions of progressively lower solute density, as shown by the contours in Fig. 2. There is no bias for the selection of Q compared to the non-solute ions, as they are selected by the same criterion. A resulting profile of the concentration of Q in each shell can be produced. Fig. 3a shows that for a RSS the concentration of Q in each shell fluctuates around the total concentration of solute.

The matrix concentration and hence Ψ can be calculated for a single dataset sampling, however the accuracy and precision is improved by making multiple dataset samplings and combining the results into a single summed concentration profile.

The concentration profile resulting from increasing d_{max} and using an inclusion step with $d_{inc} = d_{max}$ to select solute ions and non-solute ions respectively from a RSS without dataset sampling and labelling solute as Q, is shown in Fig. 3b. There is a bias towards the selection of solute ions for small values of d_{max} and a subsequent lower concentration at larger d_{max} values. The maximum separation algorithm indexes the data from regions of close proximity solute ions to regions of disparate solute ions. It is expected that for small d_{max} values the concentration of solute ions is high as it is the high solute ion concentration regions which are selected. A bias exists between selection of solute ions and non-solute ions from the reconstruction, as the criteria for their selection are different. The dataset sampling method is used because a method is needed which indexes the dataset, from regions of high solute density to low solute density, but which does not bias for selection of one ionic species over another.

Shells of progressively lower solute density are selected by increasing the selection parameters d_{max} and d_{inc}, however it is desirable to have each shell contain a similar number of ions. Using linear steps in d_{max} leads to unevenly sized shells. By using quantiles from a histogram of 1st nearest neighbours distances for all ions in the dataset to the nearest solute ion, a sequence of d_{max} values can be computed which will select shells which contain roughly the same number of ions. The exact number of ions in each shell will vary slightly due to dataset sampling. The concentration profile of Q in each shell can now be plotted against the fraction of the total ions in the dataset, f, which is more illustrative than the d_{max} parameter.

The shell beyond which the concentration is considered to be uniform and only due to the matrix now needs to be assessed. Here the cut-off point is decided by comparing the concentration of Q ions in a selected shell to the concentration of Q ions in the residual matrix from which they were selected. The residual matrix is all the sampled ions not selected as part of previous higher non-sampled solute density shells. Once the concentration of Q ions in a shell drops below that of the residual matrix, this shell and the residual matrix are considered to be confirmed as matrix (Fig. 4).

A confidence interval in this measurement of the matrix concentration can be generated by considering the counting statistics. The number of ions in the confirmed matrix, N_m will be dependent on what fraction of the total ions in the dataset, N_t, are confirmed as matrix, $(1 - f_c)$, the sampling fraction, q, and the number of repeated samples made, n.

$$N_m = nqf_cN_t \tag{3}$$

There will also have been a measured number of solute ions within the confirmed matrix, N_{ms}, leading to an estimate of the matrix concentration which is derived from $c_m = Nms/N_m$. The confidence interval

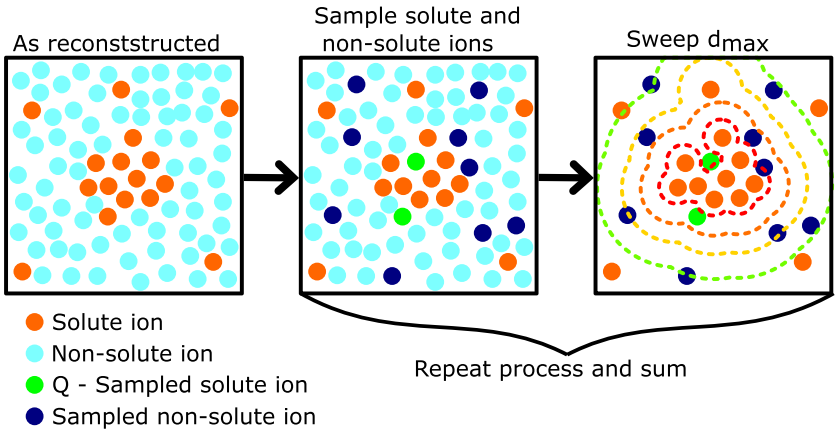

Fig. 2. Schematic representation of the process of data sampling used to remove selection bias between solute and non-solute ions. Solute ions and non-solute ions are randomly sampled. Sampled solute ions are re-categorised as Q. Unsampled non-solute is temporarily discarded. Q and sampled non-solute ions are then selected by the same inclusion method without bias around clusters defined by the unsampled solute.

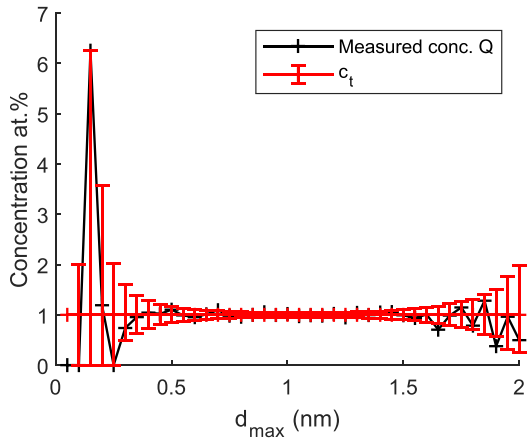

(a) No selection bias between solute and non-solute ions, by use of dataset sampling.

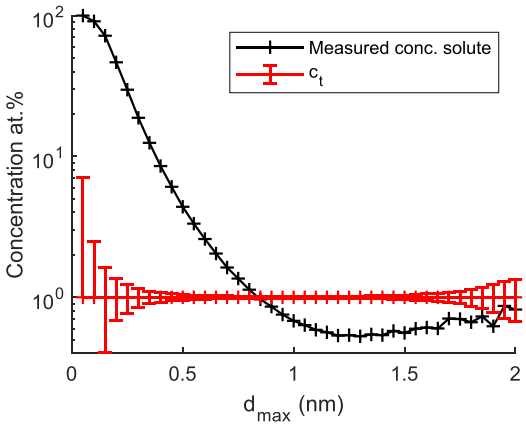

(b) Selection bias between solute and non-solute ions.

Fig. 3. Concentration profiles with and without the use of dataset sampling and recategorising of solute ions as Q ions. a) Concentration of Q (sampled solute ions; Fig. 2) selected from a RSS. Both Q and non-solute ions selected with $d_{inc} = d_{max}$. Concentration matches expected, with no selection bias. Concentration plotted on a linear scale. b) Concentration of solute selected from a RSS in shells produced by increasing d_{max} by increments. Non-solute ions selected with $d_{inc} = d_{max}$. Concentration plotted on a logarithmic scale. Error bars shown for the total concentration of the RSS, c_t, are a 95% confidence interval for binomial selection, with a fixed rate c_t and sample size equal to the number of ions selected in that shell.

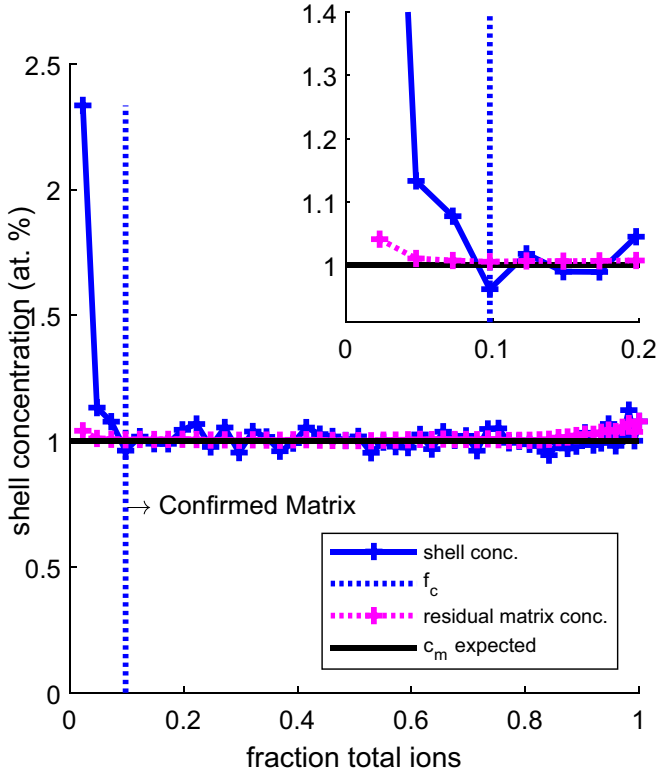

Fig. 4. Concentration of Q ions selected in progressive shells and the remaining concentration of Q within the unselected residual matrix for a synthetic dataset. The concentration of Q in the matrix (magenta) decreases as more Q is selected as part of the clusters. Shells beyond the point at which the concentration of Q in a shell falls below that of the residual matrix (indicated here by the dashed line) are defined as confirmed matrix. f_c is the fraction of ions selected as cluster overlapped with matrix, while $1 - f_c$ is the fraction of ions confirmed as being only matrix. The expected matrix solute concentration, c_m is also shown. (For interpretation of the references to colour in this figure legend, the reader is referred to the web version of this article.)

in the estimate comes from treating c_m as an estimate of a true binomial rate (Eq. (4)). In this work we use the Wilson-Score interval [25] method for estimating the confidence interval, which is more appropriate for small samples and skewed distributions, which are inherent to APT data analysis, than making a normal distribution approximation which is widely applied in APT data [26] and implemented in commercial software. A value of $z = 1.96$ leads to a 95% confidence interval, which is implemented here.

$$\left(c_m^-, c_m^+\right) = \frac{c_m + \frac{z^2}{2N_m} \pm z\sqrt{\frac{c_m(1-c_m)}{N_m} + \frac{z^2}{4N_m^2}}}{1 + \frac{z^2}{N_m}} \tag{4}$$

Repeated dataset samplings can improve the precision of the method; however the precision is limited by the original dataset size, and as such the product, nq, takes a maximum value of 1 in the calculation of N_m for Eq. (4). This confidence interval captures the statistical confidence based on the number of observations, and does not consider systematic influences. Potential systematic error could include, inclusion of concentration profile peak tail or APT artefacts arising from factors such as preferential evaporation, among other effects. These factors will be discussed further in later sections.

So far only a binary solute and non-solute system has been considered. The point excess of different ions which make up the non-solute can also be calculated via this method. Similarly, more than one ionic species can be used to define the solute. Cross-correlation of the point excess of a species where multiple different chemical species are separately used to define the solute clusters could provide interesting insights into data to investigate cases where it is suspected more than one type of solute cluster is forming.

3. Application to synthetic datasets

3.1. Creation of synthetic datasets

Synthetic data, simulating that typically generated by an APT experiment, where the characteristics of the solute clusters are known and can be controlled, were used to test the calculation of point excess solute. Synthetic datasets were created using the open source software posgen [27]. The synthetic clusters are spheres containing spatially

random solute and non-solute ions, where there is no correlation between the spatial positions of the ions. These are then placed within a spatially random matrix; Fig. 5. The target concentration for each cluster and the matrix is set beforehand, though the actual composition will vary about this target value. Clusters are placed such that they do not overlap with another cluster before the application of positional noise, but are otherwise positioned randomly. Additionally in some datasets clusters where placed so that they did not overlap with the dataset edge before application of noise (A.1). The positional noise applied is a Gaussian blur of equal amount for each direction.

The synthetic datasets contain 4 types of ion before the selection of Q ions: cluster solute; matrix solute; cluster non-solute; matrix non-solute (Fig. 5). Cluster solute and non-solute are contained within the spherical cluster regions before the application of positional noise. The number of these ions is used to calculate the synthetic matrix concentration, synthetic cluster concentration, synthetic dataset concentration and expected point excess; there is no consideration of the ions position after the application of positional noise.

$$\Psi_n \text{ expected} = 1 - \frac{\text{synthetic matrix concentration}}{\text{synthetic dataset concentration}} \tag{5}$$

3.2. Effect of different cluster characteristics

Fig. 6 shows the measured value of Ψ_n against the expected value for a range of synthetic data conditions, which are summarised in Table A.1. For these datasets a sampling fraction of 0.1 was used, with 10 repeats of sampling per dataset and 50 shells per dataset. Error bars are a 95% confidence interval in Ψ_n measured, which is derived from the same confidence interval in c_m (Eq. (4)).

In general the value of Ψ_n is recovered well and where a parameter is varied such that it changes the expected value of Ψ_n the same trend is

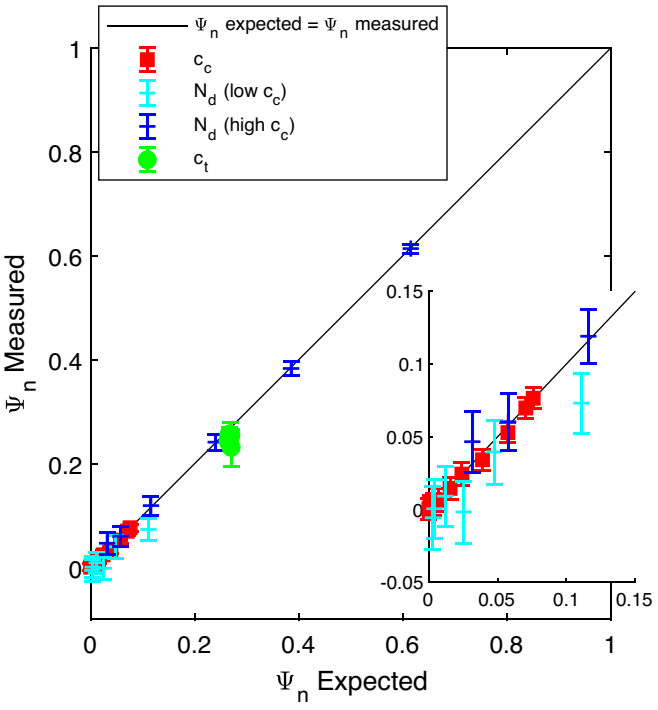

Fig. 6. Measured and expected values of Ψ_n for a range of synthetic datasets. There are four sets of synthetic datasets within which one parameter has been altered. Full synthetic dataset parameters given in Table A.1. c_c, cluster solute concentration varied; N_d, cluster number density varied (two sets with different cluster solute concentration); c_t, total solute concentration varied, with no change in partitioning behaviour.

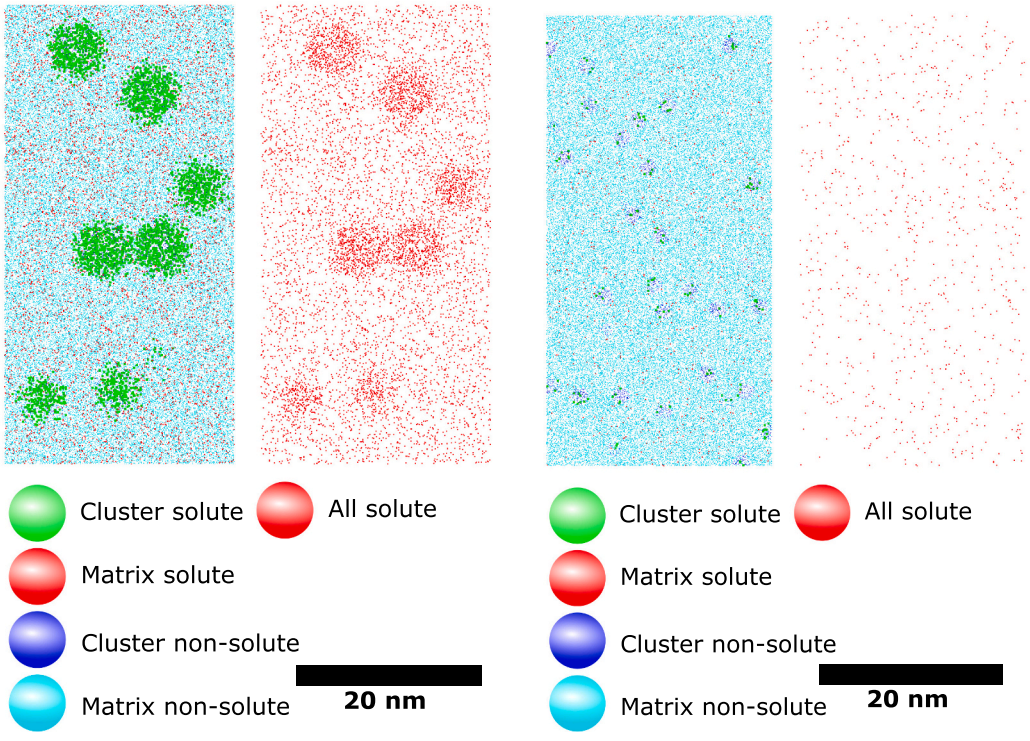

(a) 3 nm radius, 37 at.% solute clusters in a 7 at.% solute matrix

(b) 1 nm radius, 5 at.% solute clusters in a 1 at.% solute matrix

Fig. 5. 2 nm thick slices from atom maps of two synthetic datasets containing solute clusters with different cluster characteristics. For each dataset the left hand panel shows all atoms from the synthetic clusters and synthetic matrix, both solute and non-solute atoms. The right hand panel shows only solute, with no distinction between cluster solute and matrix solute.

observed in the measured data. For the datasets where cluster solute concentration was varied (red squares) the error bars are narrower, due to the larger dataset size used and greater counting statistics. When a high number density of low solute concentration clusters are added, there is an underestimation of Ψ_n, as can be seen for one of the datasets in the insert in Fig. 6. This comes from insufficient ability to resolve the original matrix concentration, even without the application of positional noise, as was the case for this dataset. The peak tail from the shell concentration profile is selected as being part of the confirmed matrix and cluster solute ions are found in even the lowest solute density shells. The impact of this scenario can is discussed further in the next section.

3.3. Effect of positional uncertainty

In an actual APT experiment the degree of blurring of the matrix-cluster interface, coming from the imperfect reconstruction of atomic positions, is likely to be unknown. It may also vary between different datasets of the same material and analysis conditions, or within a dataset if the electric field changes. A Gaussian blur on the position of every ion in the synthetic dataset has been used to simulate the uncertainty in the reconstructed ion positions. Gaussian blurs with different standard deviations, σ, were applied to two conditions, high and low solute concentration clusters and the results shown in Fig. 7.

For the high solute concentration clusters the measured value of Ψ_n is consistent with the expected value for positional uncertainty where σ is less than or equal to half the cluster radius. For standard deviations greater than half the cluster radius, the positional uncertainty leads to an underestimation of Ψ. For the low solute concentration clusters, much less positional uncertainty is required to prevent the correct identification of clusters due to the lower original contrast.

The concentration profiles produced for the datasets with $\sigma = 1.5$ nm and 3 nm with the 50 at.% solute clusters are shown in Fig. 8. It is clear from these figures why the value of Ψ is underestimated and c_m overestimated. With $\sigma = 1.5$ nm, there is overlap between solute atoms originally from different clusters and with the original matrix, and the expected original matrix concentration is not resolved. This is the situation shown by the red dashed lines in Fig. 1, where inhomogeneity of solute is still observed, but cannot be quantified by the point excess. Further blurring makes separation of the original regions impossible and the dataset appears to be a RSS (Fig. 7). The precise level of positional uncertainty needed to cause the matrix to not be resolved and underestimation of Ψ will depend on the solute cluster characteristics; the concentration contrast and number density.

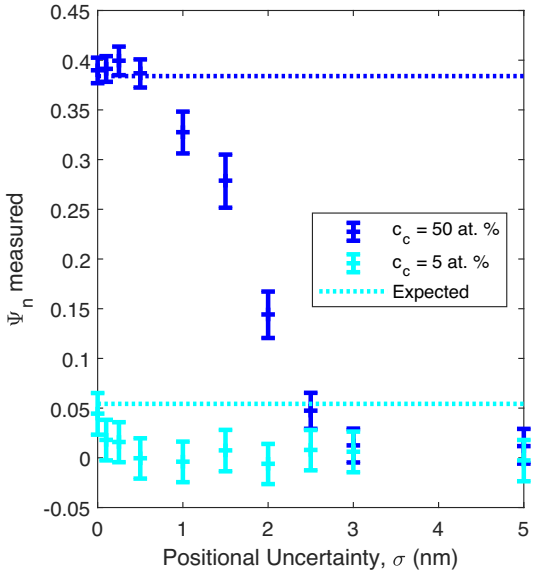

Fig. 7. Measured value of Ψ_n, for two cases with the same; matrix concentration (1 at.% solute), cluster number density (3.2 $\times 10^{-3}$ #nm-3) and cluster size (1 nm radius). In one case the clusters contain 5 at.% solute the other 50 at.%. Gaussian positional uncertainty with varying standard deviation, σ, has been applied. There were 10 repeats per dataset, the sampling fraction was 0.1 and there were 50 shells used. Error bars are a 95% confidence interval based on the confirmed matrix. High levels of positional uncertainty lead to underestimation of Ψ.

From these observations it is concluded that the measurement of point excess solute provides an accurate quantitative result when there are sufficient regions in the datasets which have the original matrix composition and when there is enough concentration contrast and spatial separation between the two regions for the maximum separation method to identify these regions. This has been tested on synthetic data down to a contrast difference of 5 at.% solute clusters in a 1 at.% solute matrix, which is a much lower contrast than is often considered in APT analysis.

In the instance where the dataset appears to be close to a RSS, with no measured point excess solute, this could be due to poor resolution and identification of features by the maximum separation algorithm, due to low contrast and/or spatial aberrations, or a genuine lack of segregation in the dataset. Detection of zero excess does not preclude segregation below the detection limit. The other case when Ψ is underestimated (and thus c_m is overestimated) is when segregation is still identified, but no matrix has been resolved. This can be assessed from observing the produced concentration profile, and assessing if the fit of a region of fixed matrix concentration is reasonable, or if as seen in Fig. 8a there is a continually decreasing concentration profile. In such cases, the value of Ψ calculated can still be used as a lower bound on the true value. It should be noted that the ability to assess when the limit of this method has been reached is an important improvement provided by this method.

It is hard for this method to overestimate the excess solute clustering, instead underestimation is more likely, due to the methodology not resolving the original matrix concentration, in a situation of high positional noise and/or low original contrast. Although not discussed here the sampling fraction and number of shells will affect the appearance of the concentration profile and in particular the computation time. These factors are discussed in more detail in the supplementary material.

3.4. Considerations for actual APT data

Actual APT datasets can differ in composition between datasets due to artefacts introduced by the evaporation process and not genuine variation in material composition. For example, the total composition of a dataset may vary from the true composition of the sample due to preferential off pulse evaporation of one or more elements. A systematic loss of one element, such that cluster concentration, matrix concentration and total concentration of that element are all decreased by the same factor, does not change the value of Ψ_n. Macro-segregation and micro-segregation within bulk samples can also lead to different APT specimens having different local solute concentration. A difference in local chemistry could affect the local solute partitioning behaviour. Such changes will be measured as a difference in the point excess and can be linked to local solute concentration if no systematic error in composition is suspected.

Field evaporation effects can further complicate the situation. If the evaporation behaviour of the two regions is different, it can affect in what ionic species elements are evaporated (i.e. complex ion formation) as well as the ion charge state, which in turn affects the degree of overlap between peaks of same and/or similar mass-to-charge-state ratio. It should be noted that this problem is not limited to this technique however and should be a general consideration when trying to measure the compositions of different regions within APT datasets. Application of mass to charge-state overlap solving for each shell [28] has the potential to also be applied to point excess solute calculations and reduce these effects.

Some portion of the ions ranged as solute ions will likely be due to

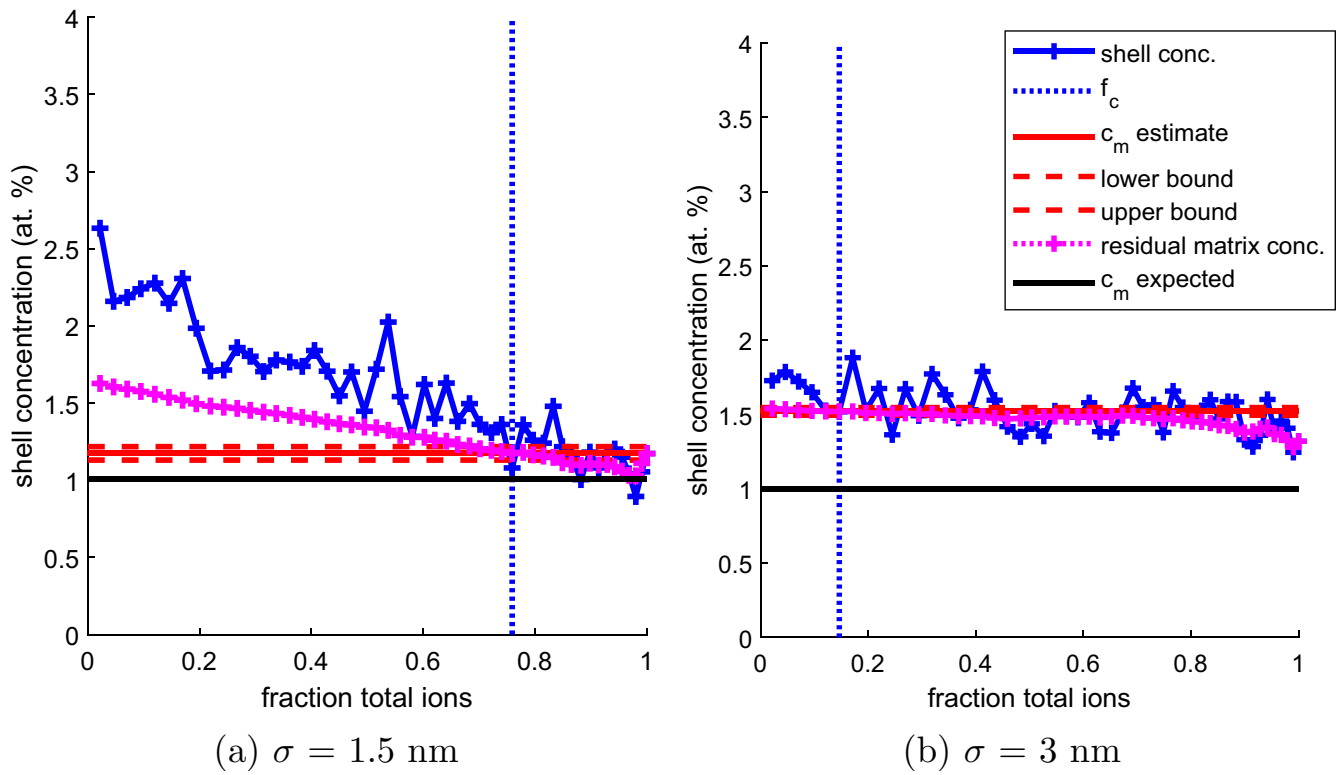

Fig. 8. Shell concentration profiles for high solute concentration clusters dataset shown in Fig. 7, with different levels of Gaussian noise. In both cases the matrix concentration was overestimated.

background noise [29,30]. If these false positive ions are not associated with the solute in the dataset and are distributed without spatial correlation throughout the dataset the increase in matrix and cluster solute concentration will be the same.

This will thus not change the value of Ψ but would decrease the value of Ψ_n. As different datasets may have different levels of background noise it is important to consider this effect. By normalising Ψ by the background corrected counts of solute ions, instead of the as-ranged value, the effect of background noise is removed. All values of Ψ_n quoted in this work for actual experimental APT data are normalised by the background corrected counts. Background correction is performed using Atom Probe Lab [31]. A global background is fitted to the mass spectrum based on the noise level at a lower mass than any observed peaks and a local background is fitted at each ranged peak to account for peak tails overlapping with neighbouring peaks [32].

There is no simple correction however if the background counts are not uniformly distributed in the dataset. A difference in background concentration between the matrix and another region can be caused by multiple effects. Background arising in one peak from overlap with the tail of another lower mass-to-charge-state ratio peak could be segregated to one region as the lower mass-to-charge-state ion is segregated to that region. High field precipitates can lead to low density regions in the dataset [33] which will appear to have a higher concentration of background if the background is of uniform density. Non-uniformity of noise from beginning to end of dataset can also occur due to changes in the ion flux rate [34]. Consideration of whether there is a strong non-uniformity in background is important for accurate quantitative results as with other APT data analysis methods.

It has been discussed, how for synthetic data, a uniform matrix concentration may not be identifiable due to a combination of low contrast between clusters and matrix regions and/or positional noise. In genuine APT datasets a uniform matrix concentration may not be identifiable, due to genuine solute segregation in the dataset, which does not lead to a region of uniform matrix concentration. Two such physical examples are, the early stages of a spinodal decomposition or a microstructure of solute clusters surrounded by a matrix region with a gradient in solute concentration due to diffusion. In such cases the solute concentration profiles produced by this method may inform as to the nature of the solute segregation, but the calculation of the point excess solute does not describe the system well and other metrics are needed.

4. Case study: naturally aged solute clusters in Al-Mg-Si

Two Al-Mg-Si-(Cu) alloys are used as a case study to demonstrate the application of the point excess solute calculation. A high Cu variant, alloy H, and low Cu variant, alloy L, of the same alloy were used, with compositions shown in Table 1. The alloys were aged at room temperature after quenching from an above solvus heat treatment, also known as and referred to here as natural ageing (NA). NA times ranged from 459 s to 76 weeks, before APT needles were prepared via standard two stage electropolishing techniques [35,36]. Work by Dumitraschkewitz et al. [37] has shown that once the nanoscale APT specimen has been formed, NA is halted at the apex of the specimen due the annihilation of quenched in excess vacancies, caused by the high surface area to volume ratio at the tip of the APT specimen. Hence, the amount of NA received by the specimens was taken to be the time between quenching and electropolishing. Further details of the methodology can be found in the supplementary material.

NA is of interest in Al-Mg-Si-(Cu) alloys as it is known to detrimentally affect the alloys response to subsequent artificial ageing, which has been related to the formation of solute clusters during NA [38–41]. Some

Table 1
Nominal compositions of alloy H and alloy L in at.%.

	Mg	Si	Cu	Al
Alloy L	0.6	0.6	0.1	Bal.
Alloy H	0.6	0.6	0.3	Bal.

APT studies [37,42] have shown that there is little or no formation of solute clusters after short amounts of NA. This work aims to build on these results and quantify the solute segregation over a sequence of NA times and investigate the effect, if any, Cu has on the solute clusters that form, as it has been shown that Cu can reduce the detrimental effect of natural ageing [43,44].

Previous studies on NA solute clusters in Al-Mg-Si-(Cu) alloys often use the maximum separation method for cluster identification [2]. As discussed in the introduction, this method requires user defined parameters, which can greatly affect the measured results and the choice of parameters is non-trivial [15], particularly for the small solute clusters expected in these alloys no appropriate parameters may exist [10]. As such these alloys are a good candidate for a trial of the point excess methodology.

Representative atoms maps from the low Cu alloy L, for a selection of ageing times and the three major solute elements, Mg, Si and Cu, are shown in Fig. 9. It can be observed qualitatively that there is more solute segregation in the dataset from the material subject to 33 weeks of NA than the shorter NA times.

Solute concentration profiles were produced for both alloys using the dataset sampling method (Fig. 10). For both Mg-to-Mg and Si-to-Si concentration it can be seen that the segregation increases with NA time. For the Si-to-Si concentration profiles (Fig. 10c and d), in the majority of datasets, the concentration of Si continued to decrease as d_{max} was increased. Either, the maximum separation method has failed to resolve cluster and matrix regions, due to the a lack of contrast and blurring between clusters and matrix in the measured dataset, or the Si is not distributed in discrete particles contained in a uniform matrix. Although the Si-to-Si segregation cannot always be quantified by the point excess solute statistic, Ψ, the concentration profiles do show there is Si-to-Si segregation in all the measured datasets and the values presented in Fig. 11d represent a lower bound on the point excess solute.

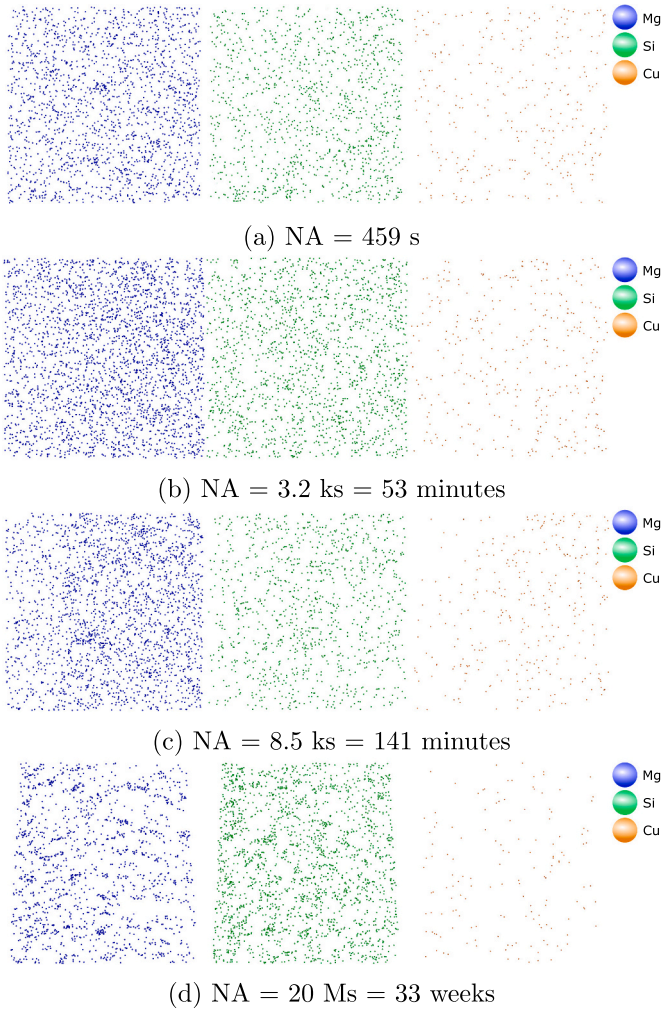

Fig. 9. APT Atom maps depicting the distribution of Mg, Si and Cu at selected room temperature ageing times for the low Cu alloy. All maps are 50 × 50 × 5 nm sections of reconstructed APT data.

The point excess solute calculation method was applied in order to quantify the level of segregation in both the low Cu alloy and in the high Cu variant. Calculations have been made with both Mg and Si as the target solute ion and are shown in Fig. 11 for the four Mg and Si combinations.

There is little Mg-to-Mg clustering at the shortest NA times (Fig. 11a). In two datasets after 30–60 min, one for each alloy, there is zero measured point excess. The lack of clustering in these datasets was confirmed also by comparison of the Mg—Mg 10th nearest neighbour histograms of the measured data and a relabelled version of those datasets. These histograms can be found in the supplementary material. The amount of excess Mg then increases approximately logarithmically with ageing time. There is no evidence that the segregation of Mg reaches an equilibrium in natural ageing the time span measured, the fraction of excess Mg continues to increase after months of NA. No clear difference in the behaviour of Mg—Mg clustering between the low and high Cu variants is observed.

The fraction of Mg in excess around Si follows very closely the fraction in excess around itself; Fig. 11b. The fraction of Si in the vicinity of Mg follows a similar trend to the Mg segregation, with very little excess at short NA times, increasing after 60 min, and continuing to increase with further ageing. For Si—Si segregation, although the value is a lower bound, at short NA times (under 20 ks = 6 h) the Si—Si excess is much greater than the excess Si around Mg (Fig. 11d and c). These observations imply that at NA times under 20 ks (6 h) there is Si—Si segregation that is not associated with Mg. Whereas the Mg—Mg segregation and Mg around Si segregation match so closely that all Mg clustering is likely associated with Si.

Further to these observations the excess fraction of Cu around Mg and Si was calculated and is shown in Fig. 12. No Cu segregation to Mg is observed for NA times under 200 ks (56 h)(Fig. 12a), while some Cu segregation to Si is observed (Fig. 12b). This would suggest that the Cu is segregated alongside the Si—Si segregation, which is also uncorrelated with Mg.

Si and Cu have been shown in other studies to segregate to ⟨111⟩ crystallographic poles during field evaporation [45,46]. This artefact was also observed here and these regions of the datasets were removed before clustering analysis (see supplementary material). Using a combined finite element and molecular dynamic simulation, Oberdorfer et al. [45] modelled the behaviour of Cu under field evaporation for a binary Al—Cu alloy. Though the Cu primarily segregated to the ⟨111⟩ poles, the distribution of Cu remaining in other regions of the tip was predicted to be non-uniform, primarily due to greater movement of Cu away from certain areas on the tip surface during the simulation.

Oberdorfer et al. also performed density functional theory (DFT) calculations of the bond energy between Al and Cu. In their model Cu segregation is caused by the bond energy sequence Cu—Cu > Al—Cu > Al—Al. This leads to retention of Cu on the surface of the tip during evaporation which then relaxes into the vacancies left by preferentially evaporated Al. The modelling was for the behaviour of Cu, however Si is predicted to segregate in the same manner but more strongly, as the bond energy differences are greater [45]. Stronger segregation of Si to ⟨111⟩ poles than Cu has been observed here (supplementary material) and elsewhere [46]. Delayed evaporation of Si relative to Mg has also been observed [47]. Mg however is not expected to segregate as the Al—Mg and Mg—Mg bonds are weaker than the Al—Al bond, which also agrees with the previous observations on pole segregation.

The major field induced clustering of Si and Cu is removed from the dataset by the removal of the ⟨111⟩ poles, however the effect may still

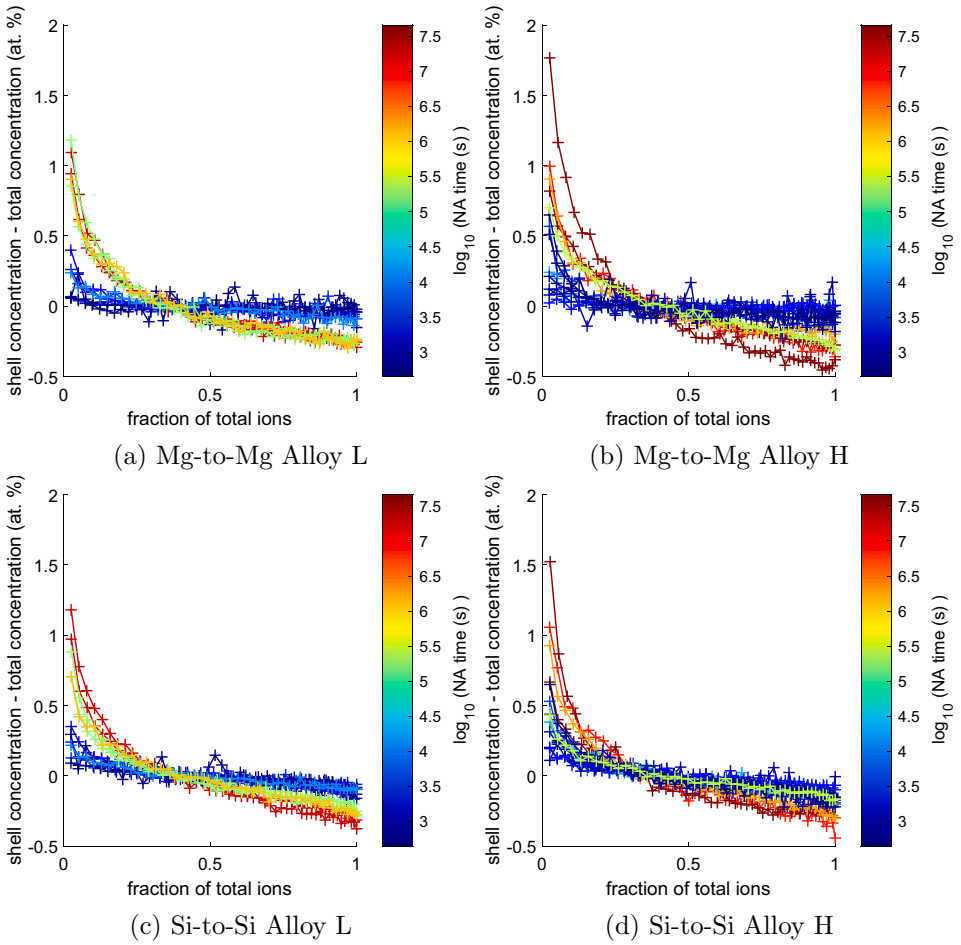

Fig. 10. Concentration profiles of solute produced using the dataset sampling method described in Section 2.1. Solute segregation increases with NA time. Sampling fraction, $q = 0.1$, number of repeats, $n = 10$. The shell concentration of solute is subtracted by the total concentration of solute for each dataset to normalise for variations in total concentration between datasets. Concentration profiles displayed include datasets of alloy L and H.

occur on a smaller scale elsewhere on the tip surface. At least some of the Si—Si and Cu to Si segregation that has been measured is likely due to a field induced effect, particularly as it has been observed without the presence of Mg which is predicted for the field induced effect. The movement of Si on the tip surface may lead to greater blurring of the Si clustering and explain why the Si—Si concentration profiles are more blurred and do not reach a plateau, but profiles for the concentration of Si around Mg do.

Models of the naturally aged clustering in Al-Mg-Si alloys have suggested that Si—Si clusters may be the first to form, with Mg segregating to these clusters after further NA [48–50]. The results presented here agree with these previous results. There is little to no Mg segregation under an hour of NA, followed by subsequent Mg association with itself and Si. It is inconclusive however if Mg-free Si clusters are forming first during NA, due to the overlay of the potential field evaporation induced Si and Cu co-segregation. This quantification and insight into the segregation behaviour is made possible by the application of the point excess solute method, while methods such as maximum separation would fail to identify such subtleties, especially if Mg and Si are used in conjunction as the target solute ions. It is clear that Cu is not influencing the rate at which NA aged solute clusters from, as the same point excess of Mg and Si are found for both alloys. The fraction of total detected Cu found in excess around the NA solute clusters is also the same between both alloys, though in the high Cu alloy this will correspond to a greater absolute concentration of Cu.

5. Conclusions

It has been discussed that in APT datasets it can commonly occur that the presence of solute segregation in the form of solute clustering can be identified, however the spatial resolution in the data can be such that the cluster characteristics; cluster concentration, volume fraction, cluster size and number density cannot be deconvolved without additional information or assumptions. However, a uniform concentration matrix may still be identifiable. In such cases of limited resolution, the point excess has been introduced as a way of quantifying solute segregation.

The point excess solute is a measure of the proportion of solute clustered in excess of the uniform matrix concentration. An adapted maximum separation approach, with dataset sampling, is a simple and effective way of indexing the dataset from ions most likely to be clustered to least, without any selection bias between different ionic species. From this a uniform concentration matrix is identified and the point excess solute calculated. The point excess solute was found to be quantitatively accurate over a range of test parameters. There is an underestimation of the expected value for the lowest solute concentration clusters investigated (5 at.% solute clusters in a 1 at.% solute matrix) or when a relatively large amount of positional uncertainty was applied, which are more challenging datasets than are often considered in APT analysis. An advantage of this method is that it also enables users to observe when a uniform concentration matrix can not be identified in the dataset. In this case, the limit of the method has been reached and accurate quantitative analysis of the data via this method is not be possible.

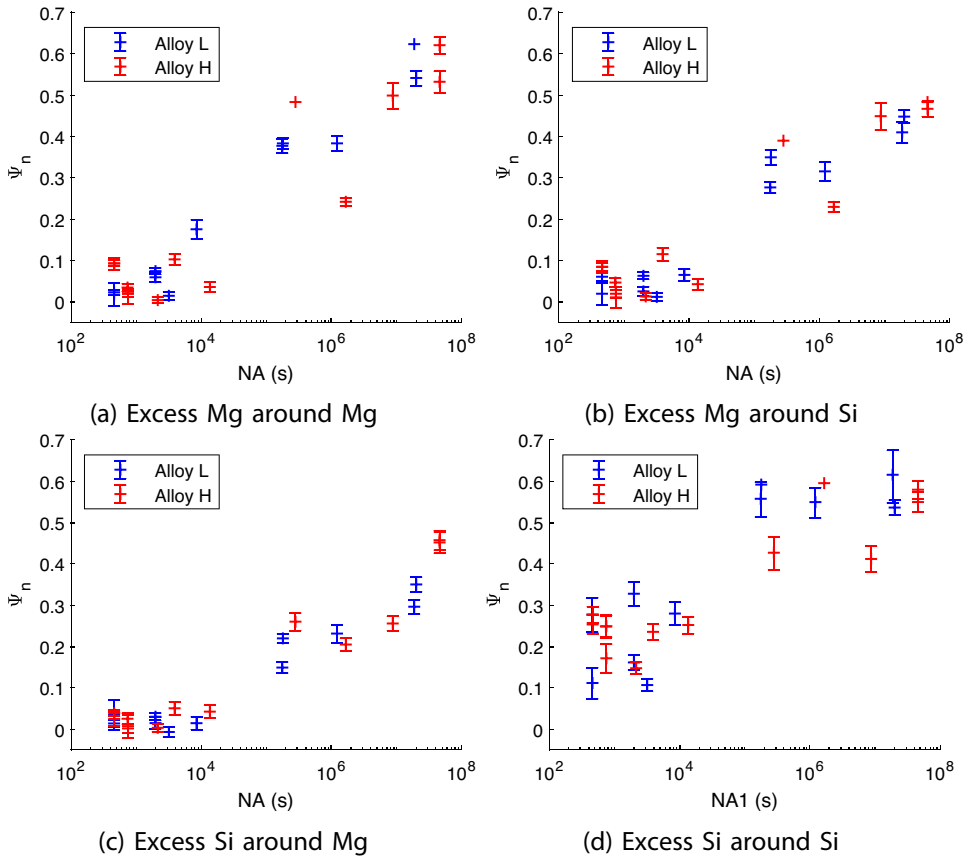

Fig. 11. The effect of NA time on Ψ_n, the normalised point excess of the target element, surrounding the chosen solute. Four combinations of solute, used to define the shells for the concentration profile, and target ion, the species of interest, are shown. For all combinations point excess increases with NA time. Background correction applied. Error bars are a 95% confidence interval.

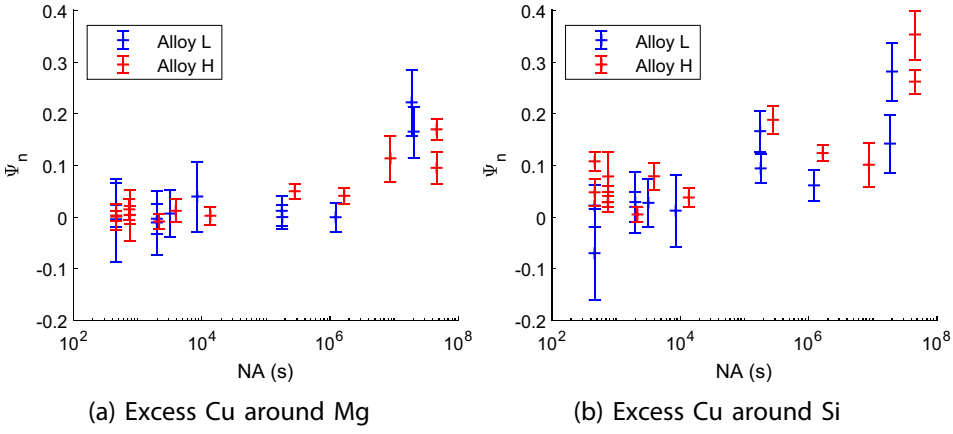

Fig. 12. The effect of NA time on point excess Cu, surrounding Mg and Si. Cu is only found in excess around Mg after long NA times, while some Cu is always found in excess around Si. Background correction applied. Error bars are a 95% confidence interval.

Naturally aged solute clusters in two Al-Mg-Si-Cu alloys, which are difficult to reliably and repeatability identify with the commonly used maximum separation algorithm, were quantified via this new method. It was seen there is little Mg solute clustering within 1 h of NA. Si segregation, free of Mg co-segregation, was observed between 8 min and 1 h of NA, however the presence of NA Mg-free Si clusters could not be confirmed due to the potential that this observed segregation is induced by the field evaporation process. A change in Cu content of the alloy is not seen to influence the point excess of Si or Mg in the NA solute clusters or the rate at which the point excess increases with NA.

Declaration of Competing Interest

The authors declare that they have no known competing financial interests or personal relationships that could have appeared to influence the work reported in this paper.

Data availability

The raw and processed data required to reproduce these findings cannot be shared at this time due to legal reasons.

Acknowledgements

The authors would like to thank Constellium for providing the materials and financially supporting this research alongside the Engineering and Physical Science Research Council (EPSRC) through studentship 1922133. The authors are grateful to EPSRC for funding of the LEAP 5000XR for the UK National Atom Probe Facility through grant EP/M022803/1.

Appendix A. Supplementary data

Supplementary data to this article can be found online at https://doi.org/10.1016/j.matchar.2023.113402.

References

[1] B. Gault, A. Chiaramonti, O. Cojocaru-Mirédin, P. Stender, R. Du-bosq, C. Freysoldt, S.K. Makineni, T. Li, M. Moody, J.M. Cairney, Atom probe tomography, Nat. Rev. Methods Primers 1 (1) (July 2021) 1–30, https://doi.org/10.1038/s43586-021-00047-w.

[2] P. Dumitraschkewitz, S.S.A. Gerstl, L.T. Stephenson, P.J. Ug-gowitzer, S. Pogatscher, Clustering in age-hardenable aluminum alloys, Adv. Eng. Mater. 20 (10) (Oct. 2018) 1800255, https://doi.org/10.1002/adem.201800255.

[3] M.K. Miller, K.F. Russell, Embrittlement of RPV steels: an atom probe tomography perspective, J. Nucl. Mater. 371 (1–3) (Sept. 2007) 145–160, https://doi.org/10.1016/J.JNUCMAT.2007.05.003.

[4] R. Verberne, S.M. Reddy, D.W. Saxey, D. Fougerouse, W.D. Rickard, D. Plavsa, A. Agangi, A.R. Kylander-Clark, The geochemical and geochronological implications of nanoscale trace-element clusters in rutile, Geology 48 (11) (Nov. 2020) 1126–1130, https://doi.org/10.1130/G48017.1.

[5] G.A. Arcuri, D.E. Moser, D.A. Reinhard, B. Langelier, D.J. Larson, Impact-triggered nanoscale Pb clustering and Pb loss domains in Archean zircon, Contrib. Mineral. Petrol. 175 (7) (July 2020) 1–13, https://doi.org/10.1007/S00410-020-01698-W/FIGURES/5.

[6] W. Lefebvre, T. Philippe, F. Vurpillot, Application of Delaunay tessellation for the characterization of solute-rich clusters in atom probe tomography, Ultramicroscopy 111 (3) (Feb. 2011) 200–206, https://doi.org/10.1016/J.ULTRAMIC.2010.11.034.

[7] P. Felfer, A.V. Ceguerra, S.P. Ringer, J.M. Cairney, Detecting and extracting clusters in atom probe data: a simple, automated method using Voronoi cells, Ultramicroscopy 150 (Mar. 2015) 30–36, https://doi.org/10.1016/J.ULTRAMIC.2014.11.015.

[8] F. De Geuser, W. Lefebvre, Determination of matrix composition based on solute-solute nearest-neighbor distances in atom probe tomography, Microsc. Res. Tech. 74 (3) (Mar. 2011) 257–263, https://doi.org/10.1002/JEMT.20899.

[9] H. Zhao, B. Gault, D. Ponge, D. Raabe, F. De Geuser, Parameter free quantitative analysis of atom probe data by correlation functions: application to the precipitation in Al-Zn-Mg-Cu, Scr. Mater. 154 (Sept. 2018) 106–110, https://doi.org/10.1016/J.SCRIPTAMAT.2018.05.024.

[10] F. De Geuser, B. Gault, Metrology of small particles and solute clusters by atom probe tomography, Acta Mater. 188 (15) (Apr. 2020) 406–415, https://doi.org/10.1016/j.actamat.2020.02.023, arXiv: 1910.10532.

[11] J. Zelenty, A. Dahl, J. Hyde, G.D. Smith, M.P. Moody, Detecting clusters in atom probe data with Gaussian mixture models, Microsc. Microanal. 23 (2) (Apr. 2017) 269–278, https://doi.org/10.1017/S1431927617000320.

[12] J. Wang, D.K. Schreiber, N. Bailey, P. Hosemann, M.B. Toloczko, The application of the OPTICS algorithm to cluster analysis in atom probe tomography data, Microsc. Microanal. 25 (2) (Apr. 2019) 338–348, https://doi.org/10.1017/S1431927618015386.

[13] G.B. Vincent, A.P. Proudian, J.D. Zimmerman, Three dimensional cluster analysis for atom probe tomography using Ripley's K-function and machine learning, Ultramicroscopy 220 (Jan. 2021), 113151, https://doi.org/10.1016/J.ULTRAMIC.2020.113151.

[14] I. Ghamarian, E.A. Marquis, Hierarchical density-based cluster analysis framework for atom probe tomography data, Ultramicroscopy 200 (May 2019) 28–38, https://doi.org/10.1016/J.ULTRAMIC.2019.01.011.

[15] E.A. Marquis, V. Araullo-Peters, Y. Dong, A. Etienne, S. Fedotova, K. Fujii, K. Fukuya, E. Kuleshova, A. Lopez, A. London, S. Lozano-Perez, Y. Nagai, K. Nishida, B. Radiguet, D. Schreiber, N. Soneda, M. Thuvander, T. Toyama, F. Sefta, P. Chou, On the use of density- based algorithms for the analysis of solute clustering in atom probe tomography data, in: J. J., P. D., and W. M (Ed.), Proceedings of the 18th International Conference on Environmental Degradation of Materials in NUclear Power Systems - Water Reactors, Springer US, 2019, pp. 2097–2113, https://doi.org/10.1007/978-3-030-04639-2_141.

[16] C.A. Williams, D. Haley, E.A. Marquis, G.D. Smith, M.P. Moody, Defining clusters in APT reconstructions of ODS steels, Ultramicroscopy 132 (Sept. 2013) 271–278, https://doi.org/10.1016/j.ultramic.2012.12.011.

[17] P. Klupś, D. Haley, A.J. London, H. Gardner, J. Famelton, B.M. Jenkins, J.M. Hyde, P.A. Bagot, M.P. Moody, PosgenPy: an automated and reproducible approach to assessing the validity of cluster search parameters in atom probe tomography datasets, Microsc. Microanal. (Sept. 2021) 1–10, https://doi.org/10.1017/S1431927621012368.

[18] L.T. Stephenson, M.P. Moody, P.V. Liddicoat, S.P. Ringer, New techniques for the analysis of fine-scaled clustering phenomena within atom probe tomography (APT) data, Microsc. Microanal. 13 (06) (Dec. 2007) 448–463, https://doi.org/10.1017/S1431927607070900.

[19] E.A. Jägle, P.P. Choi, D. Raabe, The maximum separation cluster analysis algorithm for atom-probe tomography: parameter determination and accuracy, Microsc. Microanal. 20 (6) (Sept. 2014) 1662–1671, https://doi.org/10.1017/S1431927614013294.

[20] R.K. Marceau, G. Sha, R. Ferragut, A. Dupasquier, S. Ringer, Solute clustering in Al–Cu–Mg alloys during the early stages of elevated temperature ageing, Acta Mater. 58 (15) (Sept. 2010) 4923–4939, https://doi.org/10.1016/j.actamat.2010.05.020.

[21] B.W. Krakauer, D.N. Seidman, Absolute atomic-scale measurements of the Gibbsian interfacial excess of solute at internal interfaces, Phys. Rev. B 48 (9) (Sept. 1993) 6724–6727, https://doi.org/10.1103/PhysRevB.48.6724.

[22] B.M. Jenkins, J.O. Douglas, H.M. Gardner, D. Tweddle, A. Kareer, P.S. Karamched, N. Riddle, J.M. Hyde, P.A. Bagot, G.R. Odette, M.P. Moody, A more holistic characterisation of internal interfaces in a variety of materials via complementary use of transmission Kikuchi diffraction and atom probe tomography, Appl. Surf. Sci. 528 (Oct. 2020), 147011, https://doi.org/10.1016/J.APSUSC.2020.147011.

[23] J.M. Hyde, C.A. English, An analysis of the structure of irradiation induced Cu-enriched clusters in low and high Nickel welds, in: MRS Proceedings vol. 650, Cambridge University Press, Mar. 2000, p. R6.6, https://doi.org/10.1557/PROC-650-R6.6.

[24] D. Vaumousse, A. Cerezo, P.J. Warren, A procedure for quantification of precipitate microstructures from three-dimensional atom probe data, Ultramicroscopy 95 (May 2003) 215–221, https://doi.org/10.1016/S0304-3991(02)00319-4.

[25] E.B. Wilson, Probable inference, the law of succession, and statistical inference, J. Am. Stat. Assoc. 22 (158) (1927) 209–212, https://doi.org/10.1080/01621459.1927.10502953.

[26] F. Danoix, G. Grancher, A. Bostel, D. Blavette, Standard deviations of composition measurements in atom probe analyses—part II: 3D atom probe, Ultramicroscopy 107 (9) (Sept. 2007) 739–743, https://doi.org/10.1016/J.ULTRAMIC.2007.02.005.

[27] D. Haley, Posgen 0.0.4. https://apttools.sourceforge.io/, 2020. Accessed 30/06/20.

[28] A.J. London, Quantifying uncertainty from mass-peak overlaps in atom probe microscopy, Microsc. Microanal. 25 (2) (Apr. 2019) 378–388, https://doi.org/10.1017/S1431927618016276.

[29] E. Oltman, R. Ulfig, D. Larson, Background removal methods applied to atom probe data, Microsc. Microanal. 15 (S2) (July 2009) 256–257, https://doi.org/10.1017/S1431927609095488.

[30] D. Haley, A.J. London, M.P. Moody, Processing APT spectral backgrounds for improved quantification, Microsc. Microanal. 26 (5) (Oct. 2020) 964–977, https://doi.org/10.1017/S1431927620024290.

[31] A.J. London, Atomprobelab v2.4. https://sourceforge.net/projects/atomprobelab/, 2020.

[32] A.J. London, D. Haley, M.P. Moody, Single-ion deconvolution of mass peak overlaps for atom probe microscopy, Microsc. Microanal. 23 (2) (Apr. 2017) 300–306, https://doi.org/10.1017/S1431927616012782.

[33] F. Vurpillot, A. Bostel, D. Blavette, Trajectory overlaps and local magnification in three-dimensional atom probe, Appl. Phys. Lett. 76 (21) (May 2000) 3127–3129, https://doi.org/10.1063/1.126545.

[34] D. Larson, T. Prosa, R. Ulfig, B. Geiser, T. Kelly, Local Electrode Atom Probe Tomography, 1st ed., Springer, 2013 https://doi.org/10.1007/978-1-4614-8721-0.

[35] M. Miller, A. Cerezo, M.G. Hetherington, G. Smith, Atom Probe Field Ion Microscopy, Oxford University Press, 1996.

[36] B. Gault, M.P. Moody, J.M. Cairney, S.P. Ringer, Atom Probe Microscopy. 1st ed. Springer Series in Materials Science, New York, NY, Springer New York, 2012, https://doi.org/10.1007/978-1-4614-3436-8.

[37] P. Dumitraschkewitz, P.J. Uggowitzer, S.S. Gerstl, J.F. Löffler, S. Pogatscher, Size-dependent diffusion controls natural aging in aluminium alloys, Nat. Commun. 10 (1) (Dec. 2019) 1–6, https://doi.org/10.1038/s41467-019-12762-w.

[38] D.W. Pashley, J. Rhodes, A. Sendorek, Delayed ageing in aluminium magnesium-silicon alloys - effect on structure and mechanical properties, J. Inst. Met. 94 (2) (1966) 41.

[39] S. Pogatscher, H. Antrekowitsch, H. Leitner, T. Ebner, P. Uggowitzer, Mechanisms controlling the artificial aging of Al–Mg–Si alloys, Acta Mater. 59 (9) (May 2011) 3352–3363, https://doi.org/10.1016/j.actamat.2011.02.010.

[40] G.H. Tao, C.H. Liu, J.H. Chen, Y.X. Lai, P.P. Ma, L.M. Liu, The influence of Mg to Si ratio on the negative natural aging effect in Al–Mg–Si–Cu alloys, Mater. Sci. Eng. A 642 (2015) 241–248, https://doi.org/10.1016/j.msea.2015.06.090.

[41] A. Poznak, R.K. Marceau, P. Sanders, Composition dependent thermal stability and evolution of solute clusters in Al-Mg-Si analyzed using atom probe tomography, Mater. Sci. Eng. A 721 (Apr. 2018) 47–60, https://doi.org/10.1016/j.msea.2018.02.074.

[42] P. Dumitraschkewitz, S.S.A. Gerstl, P.J. Uggowitzer, J.F. Löffler, S. Pogatscher, Atom probe tomography study of as-quenched Al-Mg-Si alloys, Adv. Eng. Mater. 19 (4) (Apr. 2017), https://doi.org/10.1002/adem.201600668.

[43] S. Wenner, C.D. Marioara, S.J. Andersen, R. Holmestad, Effect of room temperature storage time on precipitation in Al–Mg–Si(–Cu) alloys with different Mg/Si ratios, Int. J. Mater. Res. 103 (8) (Aug. 2012) 948–954, https://doi.org/10.3139/146.110795.

[44] M. Zandbergen, A. Cerezo, G. Smith, Study of precipitation in Al–Mg–Si alloys by atom probe tomography II. Influence of Cu additions, Acta Mater. 101 (Dec. 2015) 149–158, https://doi.org/10.1016/j.actamat.2015.08.018.
[45] C. Oberdorfer, T. Withrow, L.J. Yu, K. Fisher, E.A. Marquis, W. Windl, Influence of surface relaxation on solute atoms positioning within atom probe tomography reconstructions, Mater. Charact. 146 (Dec. 2018) 324–335, https://doi.org/10.1016/J.MATCHAR.2018.05.014.
[46] S. Pogatscher, S.S. Gerstl, J.F. Löffler, P.J. Uggowitzer, Atom probe tomography investigations of modified early stage clustering in Si-containing aluminum alloys, Acta Phys. Pol. A (2015) 643–646, https://doi.org/10.12693/APhysPolA.128.643.
[47] S. Jin, H. Su, F. Qian, Y. Li, G. Sha, Effects of atom probe analysis parameters on composition measurement of precipitates in an Al-Mg-Si-Cu alloy, Ultramicroscopy 235 (May 2022), 113495, https://doi.org/10.1016/J.ULTRAMIC.2022.113495.
[48] H. Zurob, H. Seyedrezai, A model for the growth of solute clusters based on vacancy trapping, Scr. Mater. 61 (2) (July 2009) 141–144, https://doi.org/10.1016/J.SCRIPTAMAT.2009.03.025.
[49] J. Banhart, C.S.T. Chang, Z. Liang, N. Wanderka, M.D.H. Lay, A.J. Hill, Natural aging in Al-Mg-Si alloys - a process of unexpected complexity, Adv. Eng. Mater. 12 (7) (July 2010) 559–571, https://doi.org/10.1002/adem.201000041.
[50] J. Banhart, M.D.H. Lay, C.S.T. Chang, A.J. Hill, Kinetics of natural aging in Al-Mg-Si alloys studied by positron annihilation lifetime spectroscopy, Phys. Rev. B 83 (1) (Jan. 2011), https://doi.org/10.1103/PhysRevB.83.014101.